

Universality in odd-even harmonic generation and application in terahertz waveform samplingDoan-An Trieu ¹, Ngoc-Loan Phan ^{1,*}, Quan-Hao Truong ¹, Hien T. Nguyen,² Cam-Tu Le ^{3,4},
DinhDuy Vu ¹ and Van-Hoang Le ^{1,†}¹*Computational Physics Key Laboratory K002, Department of Physics, Ho Chi Minh City University of Education, Ho Chi Minh City 72711, Vietnam*²*Department of Physics, Tay Nguyen University, Buon Ma Thuot City 63161, Vietnam*³*Atomic Molecular and Optical Physics Research Group, Advanced Institute of Materials Science, Ton Duc Thang University, Ho Chi Minh City 72915, Vietnam*⁴*Faculty of Applied Sciences, Ton Duc Thang University, Ho Chi Minh City 72915, Vietnam*

(Received 16 January 2023; revised 17 May 2023; accepted 10 July 2023; published 4 August 2023)

Odd-even harmonic generation contains the system's dynamical symmetry breaking, and its decoding is desirable not only in understanding physics but also for applications of dynamics extraction. In this work we discover a simple universal relation between the odd-even harmonics and the asymmetry of the terahertz (THz)-assisted laser-atomic system: atoms in a primary midinfrared laser pulse combined with a THz laser. We demonstrate numerically and then derive analytically the dependence of the harmonic even-to-odd ratio on the THz electric field. Notably, the functional form of this dependency reveals a universal scaling independent of the parameters of both the primary pulse and atomic target. This universality inspires us to propose a pump-probe scheme for THz waveform sampling from the even-to-odd ratio, accessible from conventional compact setups.

DOI: [10.1103/PhysRevA.108.023109](https://doi.org/10.1103/PhysRevA.108.023109)**I. INTRODUCTION**

Recently, high-order harmonic generation (HHG) from an asymmetric laser-target system has gained a great deal of attention since it reveals deeper structures in HHG spectra [1–11]. The most prominent feature in such symmetry-breaking systems is the emergence of even harmonics, which apparently separate them from symmetric counterparts, which emit only odd harmonics [12]. Therefore, the odd-even pattern in HHG spectra must encode the dynamical asymmetry information of the laser-target system [1–10], and thus a universal relation between them can be helpful in many extraction applications.

One route to break the spatial-temporal symmetry is adding a weaker external static electric field to the primary multicycle laser pulse [13–18]. However, to yield a visible effect, the static field needs to be impractically strong (of the order of MV/cm). Nevertheless, with recent developments of powerful terahertz (THz) sources, a quasistatic strong electric field can be engineered into the HHG process [18–27]. This THz-assisted HHG has been studied mostly in the harmonic conversion efficiency or the plateau structure [19–23] but less in other notable aspects such as odd-even harmonic spectra. Some initial estimates have been made [14,26], but a direct relation between the odd-even pattern and the asymmetry of the THz-assisted laser-atomic system has not yet been established. This relation not only is of intellectual interest but can be critical to many applications such as extracting

quantum dynamics inside atoms or molecules, manipulating electron trajectories on the attosecond timescale, or THz waveform sampling, which has been gaining attention recently [3,18,22,28,29].

Recently, it has been reported that solids under a THz field emit even harmonics that can be used to dynamically image the electric field of the THz pulse [30]. However, because of the complexity of the solids, their odd-even HHG depends on the primary laser parameters and solid targets. Hence, finding a universal odd-even harmonic rule independent of these factors is essential for a fundamental understanding of and applications in probing laser-target asymmetry.

In this work we accomplish two goals. First, we thoroughly study the response of the odd-even HHG to the variation of the THz electric field in a THz-assisted laser-atomic system. The purpose is to achieve a quantitative connection between the measurable harmonic even-to-odd ratio and the symmetry-breaking THz electric field. Interestingly, we discover a universal and simple rule for the even-to-odd ratio as a function of the scaled-THz electric field. This finding stimulates us to proceed with the second goal of proposing a general method for sampling the THz pulse waveform. The method can retrieve the time-resolved waveform with high accuracy from the harmonic even-to-odd ratio read from HHG signals at each pump-probe time delay. In this vein, we note that waveform detection is another important area of THz science that is intensively investigated in addition to its generation [18,28,29]. Within currently available methods, active matter has to be carefully chosen; thus, finding a new temporal detection scheme free from external parameters is experimentally meaningful.

*loanptn@hcmue.edu.vn

†hoanglv@hcmue.edu.vn

The rest of the paper is organized as follows. In the next section we briefly present the theoretical background, including the numerical method for solving the time-dependent Schrödinger equation that describes HHG processes and the quantum-orbit theory as the analytic foundation for the rule of the even-to-odd ratio. Section III presents three main results: numerical evidence of the universality of the even-to-odd ratio, the analytical ground of the even-to-odd ratio universality and its application in THz waveform sampling. A summary is given in Sec. IV.

II. THEORETICAL BACKGROUND

A. Numerical methods for simulating HHG

In this paper we simulate HHG data from various atoms in the combination of a linearly polarized primary mid-infrared (mid-IR) laser pulse and a collinear THz field by solving the time-dependent Schrödinger equation (TDSE) within a discretized spatial box. The numerical box size needs to be large enough to cover the electron excursions in the combined electric field. With a long-wavelength and high-power primary laser pulse, it is dramatically extended, leading to significantly expensive computational costs. On the other hand, when atoms are exposed to a linearly polarized laser, electron wave packets mostly spread along the laser polarization direction; thus, the one-dimensional (1D) model is sufficient to study the concerned HHG efficiently without a significant loss of accuracy compared to the three-dimensional model [31,32]. Additionally, a more elaborate study of the three-dimensional bare Coulomb potential model is also performed and produces the same results as those from the 1D soft Coulomb potential (see Appendix A). Therefore, in the main text, we present HHG simulated by using the 1D potential model only.

The 1D TDSE for atoms in combined laser pulses polarized along the z axis written in atomic units has the form

$$i \frac{\partial}{\partial t} \psi(z, t) = \left(-\frac{1}{2} \frac{\partial^2}{\partial z^2} + V_c(z) + V_{\text{ext}}(z, t) \right) \psi(z, t), \quad (1)$$

where $V_c(z)$ is the atomic model potential. We apply the 1D soft Coulomb potential model [32] with the form

$$V_c(z) = -\frac{Z/2}{\sqrt{z^2 + 1/4Z^2}}, \quad (2)$$

where $Z = \sqrt{2I_p}$ is the Coulomb charge, with the atomic potential ionization I_p which is equal to 0.5, 0.9036, 0.7925, and 0.5792 a.u. for H, He, Ne, and Ar, respectively, which are used in this work. This density-based model can generate HHG data that qualitatively match those from the full three-dimensional simulation [32]. It also validates single-active electron approximation when the multielectron excitation energies are remarkably larger than that of single-electron excitation, which is reasonable in small atoms and molecules [33].

The time-dependent potential couples the active electron and the external electric field in the dipole approximation as

$$V_{\text{ext}}(z, t) = zE(t), \quad (3)$$

in which the electric field $E(t)$ is combined from the primary laser pulse and the THz pulse

$$E(t) = -E_0 f(t) \sin(\omega_0 t) + E_T \cos(\omega_T t). \quad (4)$$

Here E_0 and ω_0 are the peak amplitude and carrier frequency of the primary laser, respectively, and E_T and ω_T are those for the THz electric field, respectively; $f(t)$ is the envelope of the primary laser pulse. To obtain the resolved odd- and even-order harmonics, we utilize a primary multicycle laser pulse with a trapezoidal envelope. The duration of the THz pulse is the same as that of the primary pulse.

The time-dependent wave function $\psi(z, t)$ is propagated from the atomic ground state by the split-operator method [34] with a time step of 0.01 a.u. The simulation is performed within a numerical box of size $R_m = 15r_q$, where $r_q = E_0/\omega_0^2$ is the maximum classical displacement of the electron along the z axis in the laser field. The grid spacing is 0.1 a.u. To prevent the nonphysical effects caused by the reflection of the wave function from the boundary, an absorber $\cos^{1/8}\{\pi[|z| - (R_m - W)]/2W\}$ [35] is applied, in which $W = 5r_q$ is the width of absorbing boundaries. All of the parameters are checked to ensure numerical convergence.

After obtaining $\psi(z, t)$, the laser-induced acceleration dipole is computed by Ehrenfest's theorem

$$a(t) = -\langle \psi(z, t) | \nabla V_c(z) | \psi(z, t) \rangle - E(t). \quad (5)$$

The HHG spectra are obtained by taking the modulus square of the acceleration dipole in the frequency domain

$$H(\Omega) \sim \left| \int_0^\tau a(t) e^{-i\Omega t} dt \right|^2, \quad (6)$$

where Ω is the emitted HHG frequency and τ is the time duration of the laser pulses.

B. Quantum-orbit theory

To support the goal of providing analytic insight into the even-to-odd ratio later, here we briefly recall the quantum-orbit theory inspired by Feynman's path integrals [36]. Accordingly, the induced dipole moment is a coherent superposition over all individual quantum trajectories

$$D(\Omega) = \sum_n D_n e^{-i\Phi_n}, \quad (7)$$

where $D_n(\mathbf{p}_n, t_{rn}, t_{in})$ is the temporal-spectral amplitude of the n -quantum path connecting states at a complex ionization time t_{in} and a complex recombination time t_{rn} . The harmonic phase

$$\Phi(\mathbf{p}, t_r, t_i) = \Omega t_r - S(\mathbf{p}, t_r, t_i) \quad (8)$$

contains quasiclassical action, which has the form

$$S(\mathbf{p}, t_r, t_i) = \int_{t_i}^{t_r} \left(\frac{[\mathbf{p} + \mathbf{A}(t')]^2}{2} + I_p \right) dt', \quad (9)$$

where I_p is the atomic ionization potential. The stationary condition for quasiclassical action leads to the saddle-point approximation, whose quantum trajectories noticeably contribute to harmonic generation. At this point, the classical canonical momentum is given as

$$\mathbf{p} = -\frac{1}{t_r - t_i} \int_{t_i}^{t_r} \mathbf{A}(t') dt', \quad (10)$$

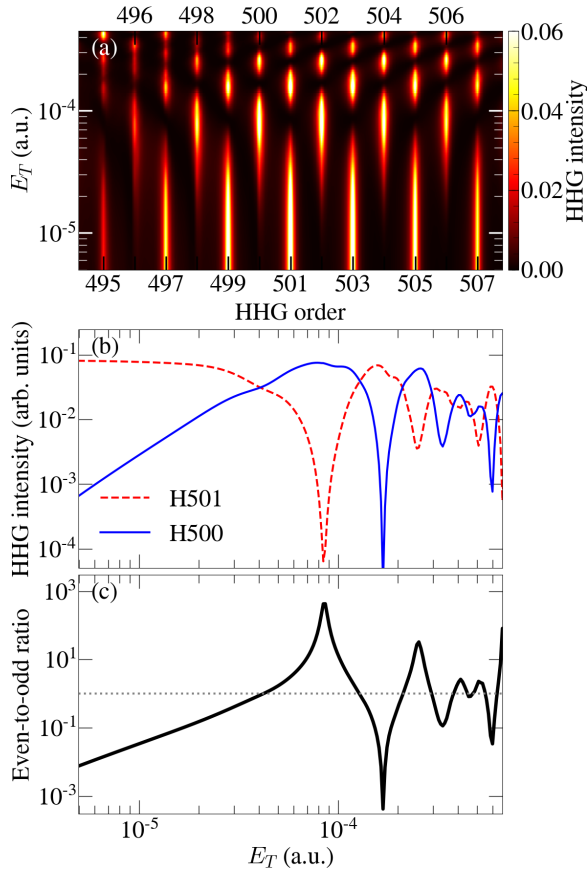


FIG. 1. Response to changing the THz electric field for (a) the intensity of resolved odd-even harmonic spectra, (b) selected odd (H501) and even (H500) harmonics at the cutoff, and (c) the harmonic even-to-odd ratio. The primary trapezoidal mid-IR laser pulse with an intensity of 2.5×10^{14} W/cm² and wavelength of 2000 nm is used for the HHG process, as well as the THz field with a frequency of 1.3 THz (231 μ m). The color bar in (a) decodes the HHG intensity in arbitrary units. The dotted horizontal line in (c) shows the unity.

where $\mathbf{A}(t) = -\int_{-\infty}^t \mathbf{E}(t')dt'$ is the vector potential of the laser field. The complex ionization t_i and recombination t_r instants can be derived from saddle-point equations, in which the derivative of the phase [Eq. (8)] vanishes.

III. RESULTS AND DISCUSSION

A. Universal response of the even-to-odd ratio to the THz electric field

We first look thoroughly into the response of resolved odd-even harmonics emitted from a hydrogen atom in the combined linearly polarized primary mid-IR laser pulse and the slowly varying THz field, as shown in Fig. 1(a). Here the HHG data are calculated by numerically solving the 1D TDSE. We consider an example of a mid-IR pulse with a ten-cycle trapezoidal envelope, an intensity of 2.5×10^{14} W/cm², and a wavelength of 2000 nm. It is clear that when the added THz field E_T is much weaker than the laser field [less than 5×10^{-6} a.u. (26 kV/cm)], the spectrum part around the cutoff is pure-odd harmonics [12]. Upon increasing the THz strength, the space-time symmetry (half-

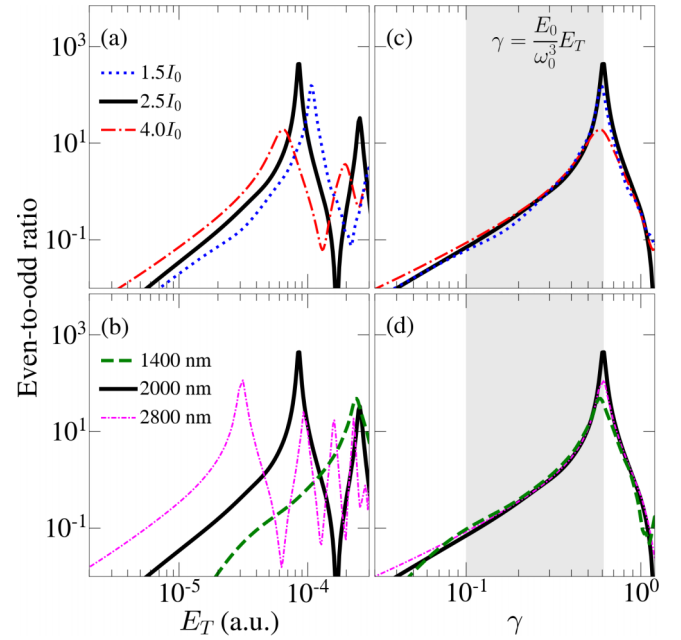


FIG. 2. Dependence of harmonic even-to-odd ratio on [(a) and (b)] a pure and [(c) and (d)] a scaled-THz electric field for a hydrogen atom in various THz-assisted primary laser pulses with (a) different intensities (fixed wavelength of 2000 nm) and (b) different wavelengths (fixed intensity of $2.5I_0$), where $I_0 = 1 \times 10^{14}$ W/cm². The gray-shaded areas in (c) and (d) highlight the region of a stable even-to-odd ratio.

period time translation combined with spatial inversion) of the original system is violated, leading to the emergence of even harmonics.

For a more focused picture, Fig. 1(b) shows the response of harmonic intensity with the THz strength for the two selected even (500th) and odd (501st) harmonics at the cutoff, denoted by H500 and H501, respectively. Their behavior can be visually partitioned into two regions. (i) For the first region, the intensity of the even harmonics gradually increases, while that of the odd harmonics is almost unchanged. (ii) After the first intersection at $E_T \approx 4 \times 10^{-5}$ a.u. (0.2 MV/cm) that indicates the equal presence of the even and odd harmonics, the second region begins with the intensity fluctuation of the odd and even harmonics around their average values. Notably, the odd and even harmonics at some specific THz field values alternatively undergo deep minima corresponding to pure-even or pure-odd spectra, as illustrated in Fig. 1(a).

Since the absolute harmonic efficiency is strongly affected by the laser field, we introduce a dimensionless quantity by taking the intensity ratio between the even harmonic and the average of the two adjacent odd ones, which is referred to as the even-to-odd ratio. The variation of this quantity with respect to the THz field is shown in Fig. 1(c). However, taking the intensity ratio does not entirely cancel the effect of the primary laser still on the THz-dependent even-to-odd ratio, as can be seen in the sensitivity to different laser intensities and wavelengths shown in Figs. 2(a) and 2(b). Specifically, the sensitivity to laser wavelength [Fig. 2(b)] is much more severe than laser intensity [Fig. 2(a)]. Remarkably, we find

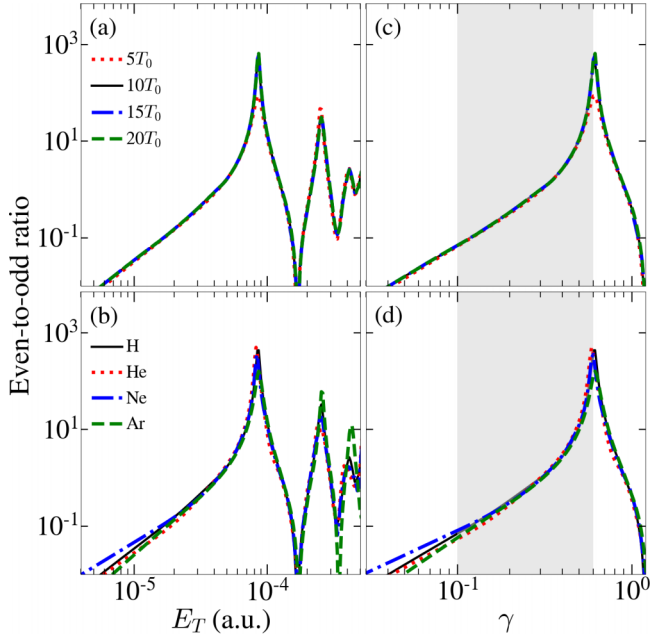


FIG. 3. Same as in Fig. 2 but with [(a) and (c)] varied number of optical cycles of the primary laser pulse (the target is a hydrogen atom) and [(b) and (d)] different atomic targets (a primary pulse of ten optical cycles is used). The primary laser has the same intensity and wavelength as used in Fig. 1.

that by rescaling the THz electric field E_T by the factor E_0/ω_0^3 as

$$\gamma = \frac{E_0}{\omega_0^3} E_T, \quad (11)$$

where E_0 and ω_0 are the primary laser's peak amplitude and carrier frequency, respectively, the data collapse quantitatively within the range $\gamma \gtrsim 0.1$ (see Fig. 2). Here the region γ below 0.1 suffers from significant numerical noise. We refer γ to as the scaled-THz electric field. We also numerically verify the data collapse with respect to the duration (5, 10, 15, and 20 cycles) of the primary laser pulse and, more interestingly, with different active atomic targets (H, He, Ne, and Ar), as shown in Fig. 3. Furthermore, the universal response as a function γ is observed not only for harmonics at the cutoff, but also for those below the cutoff with an additional condition of good phase matching in HHG experiments, as presented in detail in Appendix B.

B. Analytical ground of the even-to-odd ratio

1. Analytical derivation

The universal relation between the harmonic even-to-odd ratio and scaled-THz electric field observed numerically above motivates us to uncover its underlying physics. In this section we show that it is not accidental but can be proven rigorously by the quantum-orbit theory [36] briefly presented in Sec. II B.

Within this framework, HHG is a subcycle process in which the generation of N th-order harmonic results from the coherent interference of the attosecond bursts emitted period-

ically with half-cycle time translation

$$D(N\omega_0) \approx D_1 e^{-i\Phi_1} + D_2 e^{-i\Phi_2}, \quad (12)$$

where D_1 and D_2 are the amplitudes, and Φ_1 and Φ_2 the phases of two adjacent attosecond bursts, respectively. We assume that the THz electric field is considerably weak so that it distorts the half-cycle symmetry only of the phase but not of the magnitudes of attosecond bursts, so $D_1 \approx -D_2$. Their coherent interference gives the harmonic intensity

$$H(N\omega_0) \sim |D(N\omega_0)|^2 = 2|D_1|^2(1 - \cos\Delta\Phi), \quad (13)$$

where $\Delta\Phi = \Phi_1 - \Phi_2$ is the phase difference between the two adjacent attosecond bursts. Together with Eq. (8), it can be expressed as

$$\Delta\Phi = N\pi - \text{Re}(\Delta S), \quad (14)$$

where $\Delta S = S_1 - S_2$ is the difference between quasiclassical actions of two adjacent bursts. As a consequence, the intensities for odd and even harmonics are

$$H(N_{\text{odd}}\omega_0) \sim 2|D_1|^2\{1 + \cos[\text{Re}(\Delta S)]\}, \quad (15a)$$

$$H(N_{\text{even}}\omega_0) \sim 2|D_1|^2\{1 - \cos[\text{Re}(\Delta S)]\}, \quad (15b)$$

respectively. Taking their ratio, we have the even-to-odd ratio

$$\eta(N\omega_0) \equiv \frac{H(N_{\text{even}}\omega_0)}{H(N_{\text{odd}}\omega_0)} \approx \tan^2 \frac{\text{Re}(\Delta S)}{2}. \quad (16)$$

Equations (15) show that the additional THz field generates even harmonics via the half-cycle symmetry breaking of the quasiclassical action ΔS . Therefore, the necessary task is uncovering the quasiclassical action S of the laser-target system in the presence of a THz electric field. For more convenience in the analytical calculation, we convert the combined electric field (4) into a simpler form as

$$E(t) \approx -E_0 \sin(\omega_0 t) + E_T, \quad (17)$$

where the THz field is considered a static electric field because of its much lower frequency compared to the primary laser. Inserting into Eq. (9), the quasiclassical action can be expressed as a series of E_T as

$$S = S_0 + S_T. \quad (18)$$

Here the zeroth order describes the pure action caused by the primary laser only

$$S_0 = \frac{E_0^2}{\omega_0^3} \left(-\frac{[\sin(\omega_0 t_r) - \sin(\omega_0 t_i)]^2}{2\omega_0(t_r - t_i)} + \frac{\omega_0(t_r - t_i)}{4} + \frac{\sin(2\omega_0 t_r) - \sin(2\omega_0 t_i)}{8} \right) + I_p(t_r - t_i), \quad (19)$$

and the first-order term linearly depends on E_T as

$$S_T = E_T \frac{E_0}{\omega_0^3} \left(\frac{\omega_0(t_r - t_i)[\sin(\omega_0 t_r) + \sin(\omega_0 t_i)]}{2} + \cos(\omega_0 t_r) - \cos(\omega_0 t_i) \right) = E_T \frac{E_0}{\omega_0^3} 2 \sin \theta (\Delta\theta \cos \Delta\theta - \sin \Delta\theta), \quad (20)$$

with $\theta = \omega_0(t_r + t_i)/2$ and $\Delta\theta = \omega_0(t_r - t_i)/2$. The second-order term is omitted since the THz electric field is much weaker than the primary field, i.e., $E_T \ll E_0$.

It is clear that the zeroth-order quasiclassical action (19) is conserved after every half of an optical cycle, while the first-order one is not. This causes the phase difference of two adjacent attosecond bursts

$$\Delta S \approx \Delta S_T = 2S_T, \quad (21)$$

which gives rise to even harmonics. Substituting Eq. (21) into Eq. (16), we obtain the even-to-odd ratio as

$$\eta(N) = \tan^2 \text{Re}(S_T) = \tan^2 \left(C \frac{E_0 E_T}{\omega_0^3} \right). \quad (22)$$

For convenience, we can rewrite the even-to-odd ratio in a compact form as

$$\eta = \tan^2(C\gamma), \quad (23)$$

where γ is the dimensionless scaled-THz electric field determined by Eq. (11), which has the form in the international system of units as

$$\gamma = \frac{e^2 E_0}{\hbar m_e \omega_0^3} E_T. \quad (24)$$

The coefficient

$$C = 2 \sin \theta (\Delta\theta \cos \Delta\theta - \sin \Delta\theta) \quad (25)$$

is a dimensionless coefficient depending on harmonic ionization and recombination instants. With the assumption of $E_T \ll E_0$, these instants can easily be calculated from equations of an electron moving in the primary laser only. With laser parameters used in this study, the quantum-orbit theory gives coefficients C of high-energy harmonics (near cutoff) that is very close to the one calculated by the semiclassical simulation. Therefore, for conciseness, we simply present the estimation of coefficient C with the semiclassical approach. The calculations show that these instants are real numbers, specifically $\omega_0 t_i = 1.886$ and $\omega_0 t_r = 5.964$, which gives $C = 2.558$.

The analytical formula (23) demonstrates a direct connection between the even-to-odd ratio η (a normalized quantity characterizing the asymmetry of measurable output) and the dimensionless scaled-THz electric field γ (the normalized symmetry-breaking factor). Most importantly, Eq. (23) is free from parameters of the primary laser pulse (except implicitly in γ) and the atomic target, implying the universality of the response of the harmonic even-to-odd ratio to the scaled-THz field. In addition, this analytical expression also shows a periodic modulation of the harmonic even-to-odd ratio with the period of π/C . It alternatively undergoes maxima and minima, generating instants of the pure-even and pure-odd harmonic spectra. Based on the relation (23), we further refer to the dimensionless quantity γ as a parameter describing the asymmetric degree of the laser-target system and call it the asymmetry parameter.

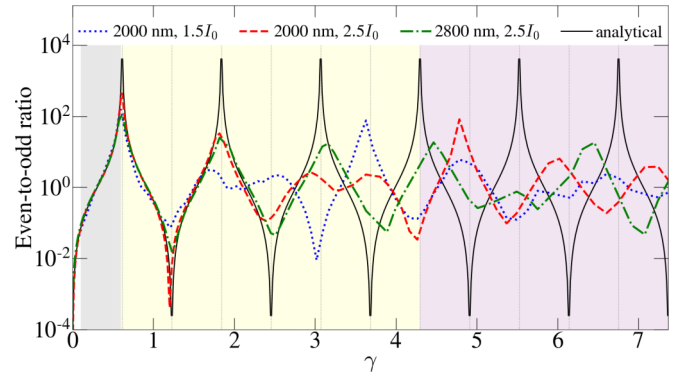


FIG. 4. Response of the harmonic even-to-odd ratio to a wide range of scaled-THz fields calculated by the analytical formula $\eta = \tan^2(2.558\gamma)$ (black solid curve) and the numerical TDSE method (dashed and dotted curves) for harmonics at the cutoff using different primary lasers enclosed in the legend. The gray-, cream-, and mauve-shaded areas cover three regions with different underlying physics mechanisms.

2. Matching numerical simulations and analytical prediction

Figure 4 shows an overall visualization of the even-to-odd ratio versus the asymmetry parameter γ for the harmonics at the cutoff. This visualization is based on the data obtained in two different ways, using analytical relations and direct numerical calculations by the TDSE method. Comparing the results of the two methods reveals three regimes with different levels of analytic-numeric agreement, implying various physical mechanisms. (i) For a small asymmetry parameter $0.1 \lesssim \gamma \lesssim 0.6$ (gray-shaded area), the analytical formula quantitatively predicts the even-to-odd ratio obtained from numerically solving the TDSE with various primary laser parameters and atomic targets. The agreement is expected within perturbative strengths of the THz field because it only modifies the electron quasiclassical motion in the continuum energy region but does not affect the ionization and recombination steps. (ii) For higher asymmetric parameters $0.6 \lesssim \gamma \lesssim 3.5\pi/C \equiv 4.3$ (cream-shaded area), the relation (23) fails to match the magnitude. Moreover, the disparity caused by the laser's parameters becomes prominent, unlike the perturbative regime. However, the reversal points (from greater than 1 to less than 1 and vice versa) still fall into the sequence of $(k + 0.5)\pi/2C$ with $k \in \mathbb{N}$. Although there are special points (at $3.5\pi/2C$ for the blue curve and $5.5\pi/2C$ for the red curve), the periodicity of the even-to-odd curves remains unchanged. The main reason is that a moderately strong THz field participates in the ionization step beyond distorting the electron quasiclassical motion. This induces the imbalance between adjacent attosecond bursts, thus reducing the interference contrast and causing irregular modulation of the even-to-odd ratio. (iii) With $\gamma \gtrsim 4.3$ (mauve-shaded area), the numerical even-to-odd ratio becomes highly disordered and the classical description (23) fails to predict both the magnitude and spacing between the reversal points. Here the intense THz field modifies ionized electrons' travel time compared to the field-free case. Additionally, intense THz fields dominate over the primary laser field in driving electron trajectories, thus altering the plateau structure of HHG spectra.

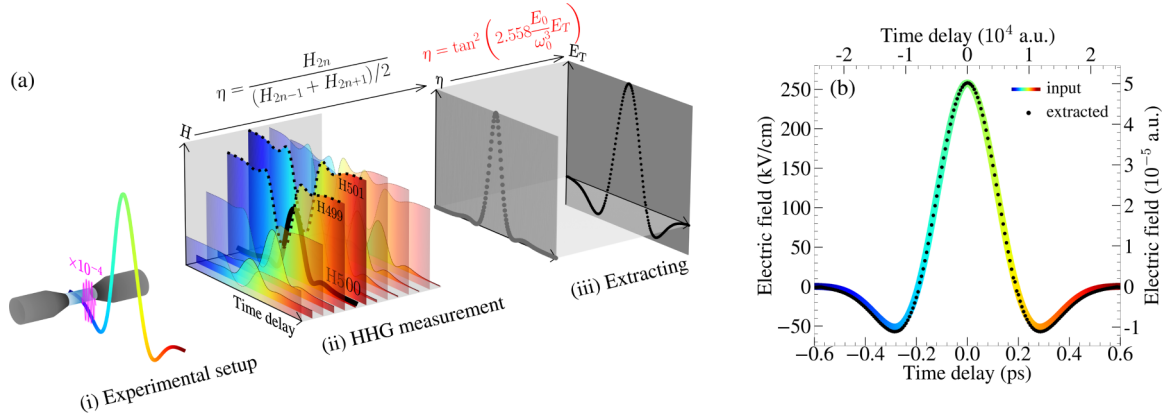


FIG. 5. (a) Proposed pump-probe scheme for sampling THz waveforms with sequential steps: (i) experimental setup with the THz pulse (pump) and a primary mid-IR laser (probe) both shinning on a gas jet, (ii) measurements of intensities of even and two adjacent odd harmonics at the cutoff region with pump-probe time delays, and (iii) extracting step, first computing the even-to-odd ratio from HHG signals and then extracting the THz electric field using the universal rule. (b) Comparison between the extracted THz pulse from simulated data (dotted curve) and its benchmark (solid curve). Five-cycle trapezoidal primary pulses with an intensity of 2.5×10^{14} W/cm² and wavelength of 2000 nm are used as probe lasers. For easier illustration, the electric-field magnitude of the primary pulse is scaled by a factor of 10^{-4} .

In short, universality manifests itself in two different aspects: the even-to-odd magnitude itself in the first region and its main oscillation frequency in the second region. We note that the predictive power of Eq. (23) is optimized [regime (i)] if the primary laser’s parameters vary in an appropriate working range (intensity within $[1.0\text{--}4.0] \times 10^{14}$ W/cm² and wavelength longer than 1200 nm (mid-IR laser)). In fact, the primary laser field E_0 must be high enough not only to ensure a low controlled ratio E_T/E_0 to avoid deforming the HHG plateau structure, but also not exceed the intensity saturation. Also, the wavelength should be long so that the asymmetry parameter γ can fall into the stable range. Appropriate laser parameters can be chosen to match available experimental spectrometer resolution. See Appendix C for details.

C. Application in THz waveform sampling

With laser parameters that optimize the validity of Eq. (23), we propose a pump-probe THz waveform sampling scheme, illustrated in Fig. 5(a). Here the THz pulse becomes the pump pulse, being probed by a delayed mid-IR laser. The two pulses meet inside a gas jet, triggering the HHG process. The odd-even HHG [Fig. 5(a) (ii)] and consequently the even-to-odd ratio [Fig. 5(a) (iii)] are recorded at each time delay. With the analytical formula (23), the waveform of the THz pulse can be easily reconstructed [Fig. 5(a) (iii)].

Figure 5 shows an example of the waveform “measurement” from simulated HHG for the THz pulse $E_T(t) = E_{T0} \exp(-\omega_T^2 t^2 / 36\pi^2) \sin \omega_T t$, with $E_T = 257$ kV/cm and frequency $\omega_T = 1.3$ THz, inspired by the pulse recently reported in [37]. The five-cycle trapezoidal primary pulses with 2.5×10^{14} W/cm² intensity and 2000 nm wavelength are used as probe lasers. The time resolution of the THz waveform sampling is related to the probe pulse duration, which is about 20 fs for the five-cycle laser pulse with three cycles in the flat part. Figure 5(b) demonstrates the validity of our proposed procedure. It indicates a good consistency between

the extracted THz waveform and the input data. We have also examined and affirmed the validity of the proposed method in sampling THz pulses with complicated waveforms, implying a broad frequency band (not shown). We note that the carrier-envelope phase of the detected THz pulse might be flipped by π since the proposed method can extract the magnitude only but not its sign.

Using the optimized universal rule can detect the THz electric field within a wide THz field range of about [20,2000] kV/cm imposed by the working range of the probing laser pulses (see Appendix C). We emphasize that the detectable range can be expanded if we use the suboptimal regime [regime (ii) of Fig. 4] of γ , looking only at its stable spacing between reversal points. We leave the details for future work.

IV. CONCLUSION

In this paper we have both numerically and analytically demonstrated the universal dependence of the even-to-odd ratio on the scaled-THz electric field (asymmetry parameter of the system). The approach to derive the universal rule in this work can be generalized to other asymmetric laser-target systems that may be meaningful in controlling electron dynamics within an attosecond timescale or extracting asymmetric factors of laser-target systems.

Based on this universal rule, we have proposed a pump-probe method for THz waveform sampling using the even-to-odd ratio, which is measurable within current compact laser setups. Unlike the previous methods for THz detection involving electronic or optical excitation of targets under THz pulse, our proposed method works on the perturbative regime in which the THz field only affects the dynamics of quasifree electrons in the continuum energy region, leading to modulation of the even-to-odd ratio, but does not directly interact with the targets. This independence of the targets and probe laser parameters makes the method feasible for detecting a wide range of THz electric fields.

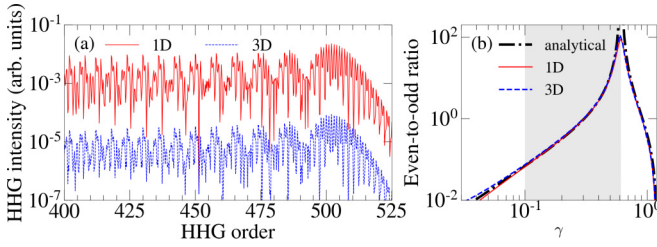


FIG. 6. Comparison of (a) HHG spectra and (b) their scaled-THz-dependent even-to-odd ratio of the hydrogen atom when employing two potential models: the one-dimensional soft Coulomb (1D) and three-dimensional bare Coulomb (3D) models. The trapezoidal primary laser pulse with a duration of five optical cycles, an intensity of 2.5×10^{14} W/cm², and a wavelength of 2000 nm is used. In (a) the THz pulse has an amplitude of $E_T = 4 \times 10^{-4}$ a.u. In (b) the analytical even-to-odd curve is given as a benchmark.

ACKNOWLEDGMENTS

This work was funded by Vingroup and supported by Vingroup Innovation Foundation (VINIF) under project code VINIF.2021.DA00031. The calculations were executed by the high-performance computing cluster at Ho Chi Minh City University of Education, Vietnam.

APPENDIX A: MODEL INDEPENDENCE OF THE EVEN-TO-ODD RATIO

In this Appendix we demonstrate that the problems of reduced dimensionality and softening Coulomb potential do not affect the even-to-odd ratio and its universality. To this end, we employ the QPROP solver [38] for numerically solving the TDSE for the 3D hydrogen atom with bare Coulomb potential in the combination of a primary laser and THz pulse as described by Eq. (4). The simulation is performed within the numerical box with the radius of $R_m = R_r + 2.5r_q + W_{\text{im}}$, in which the position of the flux-capturing surface $R_r = 20$ a.u. and the width of the imaginary potential $W_{\text{im}} = 100$ a.u. The radial grid is $\Delta r = 0.04$ a.u. The partial wave function is expanded into spherical harmonic functions up to $L_{\text{max}} = 160$. The time evolution of the wave function is propagated with a time step of $\Delta t = 0.01$ a.u. After obtaining the time-dependent wave functions, HHG is computed from the temporal acceleration dipole (5) through the Fourier transform (6).

The simulated HHG by the 3D bare Coulomb potential model and its counterpart by the 1D soft Coulomb potential are presented in Fig. 6(a), which shows their similarity regardless of the dimensionality and Coulomb-potential type. Consequently, their even-to-odd ratios are similar and coincide with the analytical prediction as indicated in Fig. 6(b). In addition, as demonstrated in Fig. 7, by employing this 3D bare Coulomb potential we also confirm the insensitivity of γ -dependent even-to-odd ratio to the changing of the primary laser's intensities and wavelength.

Furthermore, along with the simulation for atomic targets, we also examine the odd-even universality for the symmetric-molecular targets. The simulation is performed by numerically solving the TDSE for two-dimensional soft-core Coulomb potential models for N₂ and O₂ molecules. The results (not shown) show the coincidence of γ -dependent

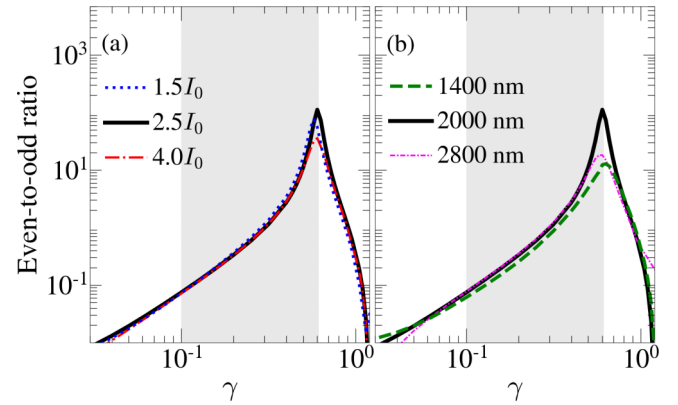


FIG. 7. Insensitivity of even-to-odd ratio versus scaled-THz electric field with a changing primary (a) laser intensity (wavelength of 2000 nm) and (b) laser wavelength (intensity of $2.5I_0$). The bare Coulomb 3D potential model of the hydrogen atom is implemented for numerical simulations.

even-to-odd ratios of molecules with those of atoms and with the analytical solutions (23).

The above evidence affirms the universality of the even-to-odd ratio despite the diverse targets and their potentials (dimensionality and Coulomb-potential type). This universality can be easily understood since the emergence of even harmonics in the THz perturbation regime [regime (i)] is caused by the distortion of the phase of two adjacent attosecond bursts, which in turn is governed by the motion of electron during propagation only and does not influence by the targets. Therefore, the analytical formula (23) does not depend on any target's and its potential's parameters as long as it is inversion symmetric. Thus, the THz-dependent even-to-odd ratio is not influenced by the potential models, including the reduced dimensionality Coulomb-potential type.

APPENDIX B: UNIVERSALITY OF THE EVEN-TO-ODD RATIO FOR HARMONICS BELOW CUTOFF

In the main text we mentioned that the universality of the even-to-odd ratio is also validated for harmonics below the cutoff in the case of a good macroscopic phase-matching condition in HHG measurement where the short electron trajectories are favorable. In this Appendix we present the evidence.

For harmonics below the cutoff, besides the inter-half-cycle interference of bursts emitted with half-cycle time translation, the intra-half-cycle interference of emission contributed from the short and long trajectories and even high-order returns of multiple rescattering also significantly modulates harmonic intensities [31,39]. Moreover, the weight contribution of long and short trajectories is strongly governed by the driven laser [31]; as a consequence, the even-to-odd ratio for these harmonics is no longer stable with the laser parameters (not shown).

A common way to avoid intra-half-cycle interference is to eliminate long trajectories with a good phase-matching setup in HHG experiments [40,41]. This macroscopic phase-matching condition can be theoretically mimicked based on a single-atom response either by coherently summing up

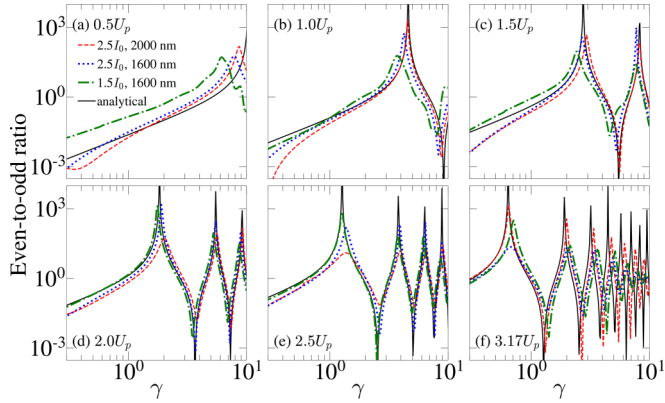


FIG. 8. Even-to-odd ratio for harmonics below cutoff versus the scaled-THz electric field γ for primary mid-IR pulses with various intensities and wavelengths when keeping only short electron trajectories in the simulation by the TDSE method. The classical simulation of scaled-THz-dependent even-to-odd ratio is exhibited by solid curves. The harmonic energy \mathcal{E} is characterized by the corresponding kinetic energy of electron K in units of ponderomotive energy U_p : (a) $0.5U_p$, (b) $1.0U_p$, (c) $1.5U_p$, (d) $2.0U_p$, (e) $2.5U_p$, and (f) $3.17U_p$.

HHG spectra calculated for a proper range of laser intensity within the laser focus [42,43] or by setting a proper absorbing boundary beyond which an absorbing procedure filters out the continuum wave packets related to long trajectories [8,10,44,45]. The latter approach is adopted in our study, where the absorber with a width of 200 a.u. is applied from $1.1r_q$ to the edge of the simulation box.

A general view of the simulated even-to-odd ratio as a function of the scaled-THz field when selecting only short electron trajectories is illustrated in Fig. 8 for different photon energies \mathcal{E} corresponding to the kinetic energy of electron K through the energy conversion $\mathcal{E} = K + I_p$. The figure shows three noticeable features. First, the behavior of the even-to-odd ratio with the scaled-THz field γ for below-cutoff harmonics is similar to that of harmonics at the cutoff. Second, it reveals a notable shift of the even-to-odd ratio as a whole towards smaller γ as the harmonic energy \mathcal{E} increases. Third, it demonstrates considerable stability of the even-to-odd ratio for below-cutoff harmonics with the scaled-THz field γ despite changing the primary mid-IR laser's parameter. However, the stability is degraded for low-order harmonics whose energy is below $I_p + 2U_p$, where U_p is the ponderomotive energy.

To justify the above observations, we implement the analytical relation (23) to simulate the even-to-odd ratio for harmonics below the cutoff. For this purpose, we first simulate the values of the coefficient C via Eq. (25) and show them in Fig. 9. Here the ionization and recombination instants are detected from classical simulation. Figure 9 shows that if only short electron trajectories are selected, the coefficient C is a one-to-one function of the electron kinetic energy K , which in turn converts to harmonic energy \mathcal{E} . Then we substitute this harmonic-dependent coefficient C into Eq. (23) and present the obtained analytical even-to-odd ratio as black solid curves in Fig. 8, showing good agreement between the numerical and analytical simulation for a wide range of scaled-THz

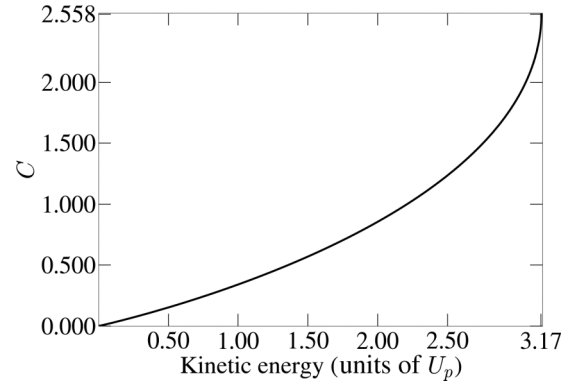


FIG. 9. Classical simulation of coefficient C versus the kinetic energy of electron K when selecting short trajectories.

electric fields. Furthermore, it explains the apparent shift of the even-to-odd ratio towards smaller γ with increasing C due to the extension of the excursion time of electrons in the region of the continuum energy as the harmonic energy \mathcal{E} increases. Moreover, from the point of view of the classical simulation, the coefficient C is independent of the primary laser's parameters, leading to the apparent stability of the scaled-THz even-to-odd ratio. However, as shown by more complex models such as quantum-orbit theory [46], the excursion time of the electron slightly depends on the primary laser parameters, especially for low-energy harmonics, which might explain their lower consistency between numerical and analytical values of the even-to-odd ratio. Therefore, we recommend implementing the even-to-odd ratio of harmonics in the high-energy plateau region or at the cutoff for the most accurate universality rule.

APPENDIX C: WORKING RANGE

We have found that in the first region with $0.1 \leq \gamma \leq 0.6$, the even-to-odd ratio versus the scaled-THz electric field is almost stable against changing primary laser parameters in an appropriate range. This universality is well described by the analytical relation (23). However, as noted in the main text, this universality is validated if certain requirements for the primary laser are met.

The first requirement is that its intensity is high enough to generate HHG and should not exceed the saturation intensity where the atomic ground state is depleted [47]. Moreover, for atoms in an intense primary laser combined with a low-frequency electric field, the ratio E_T/E_0 is a key quantity controlling the electron trajectories and, consequently, deforming the structures and properties of HHG [14,15]. To perturb the asymmetry of the laser-atomic system but not change the spectral structure of HHG, this ratio E_T/E_0 must be small (less than 0.3%); thereby, the intensity of the primary laser must be high enough to reduce the ratio E_T/E_0 . In our simulation for hydrogen atoms, the intensity varying in the range of $[1.0-4.0] \times 10^{14}$ W/cm² gives a stable even-to-odd ratio rule in the first region of the scaled-THz electric field.

The following requirement for primary wavelengths relates to the restriction of the lower and upper limits of the first universal rule, i.e., $0.1 \leq \gamma \leq 0.6$, while at the same time

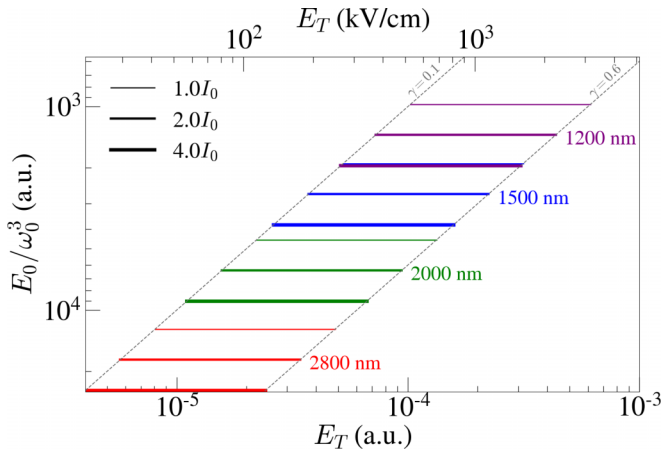


FIG. 10. Detectable range for the THz electric field E_T when using different mid-IR primary laser pulses in the appropriate working range. The detectable THz field E_T is inferred from the limitation of the stable range $0.1 \leq \gamma \leq 0.6$.

ensuring a low ratio E_T/E_0 (less than 0.3%). The analytical formula (23) hints that the primary laser wavelengths need to be long. On the other hand, longer wavelengths also guarantee that the Keldysh parameter is much less than unity; thus the primary field induces ionization within the tunneling regime [48]. Our examination shows that the mid-IR primary laser

whose wavelength is longer than 1200 nm but shorter than 3000 nm is appropriate to ensure the universality of the even-to-odd ratio versus the scaled-THz electric field.

With primary laser pulses within this working range, the THz-dependent even-to-odd ratio calculated numerically can be accurately described by the analytical relation (23) for the first universal region $0.1 \leq \gamma \leq 0.6$. Figure 10 shows that, depending on the estimated THz electric field, the appropriate primary laser's parameter should be chosen to ensure that the scaled-THz field γ falls within this stable range. This leads to the detection range of the THz field E_T within $[4 \times 10^{-6}, 4 \times 10^{-4}]$ a.u. ($[20, 2000]$ kV/cm).

We emphasize that this detectable range of the THz field can be expanded using the suboptimal regime, where only its stable oscillation period is preserved. We sketch the route utilizing this rule to detect the THz field as an outlook. By looking at the analytical formula (23), a new dimensionless quantity $\zeta = (1 - \eta)/(1 + \eta)$ can be defined as a harmonic oscillation as

$$\zeta = \cos\left(\frac{2CE_0}{\omega_0^3}E_T\right). \quad (\text{C1})$$

In practice, one can tune ζ by changing the value E_0/ω_0^3 , by scanning either the mid-IR intensity or the wavelength [49]. Afterward, the Fourier transform of this function $\zeta(2CE_0/\omega_0^3)$ gives a peak at E_T .

- [1] E. Frumker, N. Kajumba, J. B. Bertrand, H. J. Wörner, C. T. Hebeisen, P. Hockett, M. Spanner, S. Patchkovskii, G. G. Paulus, D. M. Villeneuve, A. Naumov, and P. B. Corkum, *Phys. Rev. Lett.* **109**, 233904 (2012).
- [2] Y. J. Chen, L. B. Fu, and J. Liu, *Phys. Rev. Lett.* **111**, 073902 (2013).
- [3] O. Pedatzur, G. Orenstein, V. Serbinenko, H. Soifer, B. Bruner, A. Uzan, D. Brambila, A. Harvey, L. Torlina, F. Morales, O. Smirnova, and N. Dudovich, *Nat. Phys.* **11**, 815 (2015).
- [4] P. Kraus, O. I. Tolstikhin, D. Baykusheva, A. Rupenyan, J. Schneider, C. Z. Bisgaard, T. Morishita, F. Jensen, L. B. Madsen, and H. J. Wörner, *Nat. Commun.* **6**, 7039 (2015).
- [5] C. Chen, F.-M. Guo, Y.-J. Yang, Y.-J. Chen, and S.-P. Yang, *Europhys. Lett.* **127**, 34004 (2019).
- [6] W. Y. Li, R. H. Xu, X. J. Xie, and Y. J. Chen, *Phys. Rev. A* **100**, 043421 (2019).
- [7] H. Yin, D. Liu, and F. Zeng, *Appl. Phys. Lett.* **119**, 151105 (2021).
- [8] H. T. Nguyen, K.-N. H. Nguyen, N.-L. Phan, C.-T. Le, D. Vu, L.-P. Tran, and V.-H. Le, *Phys. Rev. A* **105**, 023106 (2022).
- [9] L. He, S. Sun, P. Lan, Y. He, B. Wang, P. Wang, X. Zhu, L. Li, W. Cao, P. Lu, and C. D. Lin, *Nat. Commun.* **13**, 4595 (2022).
- [10] K.-N. H. Nguyen, N.-L. Phan, C.-T. Le, D. Vu, and V.-H. Le, *Phys. Rev. A* **106**, 063108 (2022).
- [11] X. Wang, A.-T. Le, Z. Zhou, H. Wei, and C. D. Lin, *Phys. Rev. A* **96**, 023424 (2017).
- [12] N. Ben-Tal, N. Moiseyev, and A. Beswick, *J. Phys. B* **26**, 3017 (1993).
- [13] M.-Q. Bao and A. F. Starace, *Phys. Rev. A* **53**, R3723(R) (1996).
- [14] B. Wang, X. Li, and P. Fu, *J. Phys. B* **31**, 1961 (1998).
- [15] W. Hong, P. Lu, W. Cao, P. Lan, and X. Wang, *J. Phys. B* **40**, 2321 (2007).
- [16] G. Zhao, X. Guo, T. Shao, and K. Xue, *New J. Phys.* **13**, 093035 (2011).
- [17] C.-T. Le, N.-L. Phan, D. D. Vu, C. Ngo, and V.-H. Le, *Phys. Chem. Chem. Phys.* **24**, 6053 (2022).
- [18] A. A. Silaev, A. A. Romanov, and N. V. Vvedenskii, *Opt. Lett.* **47**, 4664 (2022).
- [19] W. Hong, P. Lu, P. Lan, Q. Zhang, and X. Wang, *Opt. Express* **17**, 5139 (2009).
- [20] E. Balogh, K. Kovacs, P. Dombi, J. A. Fulop, G. Farkas, J. Hebling, V. Tosa, and K. Varju, *Phys. Rev. A* **84**, 023806 (2011).
- [21] C. Jia, J. Wang, Q.-Y. Li, F.-M. Guo, J.-G. Chen, S.-L. Zeng, and Y.-J. Yang, *Opt. Express* **23**, 32222 (2015).
- [22] X.-L. Ge, H. Du, J. Guo, and X.-S. Liu, *Opt. Express* **23**, 8837 (2015).
- [23] I. Babushkin, A. Demircan, U. Morgner, and A. Savel'ev, *Phys. Rev. A* **106**, 013115 (2022).
- [24] D. B. Milošević, *Opt. Lett.* **47**, 1669 (2022).
- [25] S. Brennecke, M. Ranke, A. Dimitriou, S. Walther, M. J. Prandolini, M. Lein, and U. Fröhling, *Phys. Rev. Lett.* **129**, 213202 (2022).
- [26] A. A. Silaev, A. A. Romanov, and N. V. Vvedenskii, *J. Phys.: Conf. Ser.* **2249**, 012004 (2022).
- [27] W. Mao, A. Rubio, and S. A. Sato, *Phys. Rev. B* **106**, 024313 (2022).
- [28] X. C. Zhang, A. Shkurinov, and Y. Zhang, *Nat. Photon.* **11**, 16 (2017).
- [29] Y. Zhang, K. Li, and H. Zhao, *Front. Optoelectron.* **14**, 4 (2021).
- [30] G. Vampa, T. Hammond, M. Taucer, X. Ding, X. Ropagnol, T. Ozaki, S. Delprat, M. Chaker, N. Thiré, B. Schmidt, F. Légaé,

- D. Klug, A. Y. Naumov, D. M. Villeneuve, A. Staudte, and P. B. Corkum, *Nat. Photon.* **12**, 465 (2018).
- [31] C. C. Chirilă, I. Dreissigacker, E. V. van der Zwan, and M. Lein, *Phys. Rev. A* **81**, 033412 (2010).
- [32] S. Majorosi, M. G. Benedict, and A. Czirják, *Phys. Rev. A* **98**, 023401 (2018).
- [33] A. Nayak, M. Dumergue, S. Kühn, S. Mondal, T. Csizmadia, N. Harshitha, M. Füle, M. Upadhyay Kahaly, B. Farkas, B. Major, V. Szaszko-Bogár, P. Földi, S. Majorosi, N. Tsatrafyllis, E. Skantzakis, L. Neoričić, M. Shirozhan, G. Vampa, K. Varjú, P. Tzallas *et al.*, *Phys. Rep.* **833**, 1 (2019).
- [34] A. D. Bandrauk and H. Shen, *Chem. Phys. Lett.* **176**, 428 (1991).
- [35] K.-J. Yuan and A. D. Bandrauk, *Phys. Rev. A* **88**, 013417 (2013).
- [36] P. Salières, B. Carré, L. Le Déroff, F. Grasbon, G. G. Paulus, H. Walther, R. Kopold, W. Becker, D. B. Milošević, A. Sanpera, and M. Lewenstein, *Science* **292**, 902 (2001).
- [37] M. Shalaby, C. Vicario, K. Thirupugalmani, S. Brahadeeswaran, and C. P. Hauri, *Opt. Lett.* **41**, 1777 (2016).
- [38] V. Tulsy and D. Bauer, *Comput. Phys. Commun.* **251**, 107098 (2020).
- [39] M. Lewenstein, P. Balcou, M. Y. Ivanov, A. L’Huillier, and P. B. Corkum, *Phys. Rev. A* **49**, 2117 (1994).
- [40] V. V. Strelkov, M. A. Khokhlova, A. A. Gonoskov, I. A. Gonoskov, and M. Y. Ryabikin, *Phys. Rev. A* **86**, 013404 (2012).
- [41] C. Jin, A.-T. Le, and C. D. Lin, *Phys. Rev. A* **79**, 053413 (2009).
- [42] T. Morishita, A.-T. Le, Z. Chen, and C. D. Lin, *Phys. Rev. Lett.* **100**, 013903 (2008).
- [43] A.-T. Le, T. Morishita, and C. D. Lin, *Phys. Rev. A* **78**, 023814 (2008).
- [44] S. Yu, B. Zhang, Y. Li, S. Yang, and Y. Chen, *Phys. Rev. A* **90**, 053844 (2014).
- [45] N.-L. Phan, K.-N. H. Nguyen, C.-T. Le, D. Vu, K. Tran, and V.-H. Le, *Phys. Rev. A* **102**, 063104 (2020).
- [46] J. Zhao and M. Lein, *Phys. Rev. Lett.* **111**, 043901 (2013).
- [47] A. D. Shiner, C. Trallero-Herrero, N. Kajumba, H.-C. Bandulet, D. Comtois, F. Légaré, M. Giguère, J.-C. Kieffer, P. B. Corkum, and D. M. Villeneuve, *Phys. Rev. Lett.* **103**, 073902 (2009).
- [48] L. Keldysh, *Sov. Phys. JETP* **20**, 1307 (1965).
- [49] D. R. Tuthill, T. D. Scarborough, T. T. Gorman, K. A. Hamer, R. R. Jones, M. B. Gaarde, K. Lopata, F. Mauger, K. J. Schafer, and L. F. DiMauro, *J. Phys. Chem. A* **126**, 8588 (2022).